Research Square

Preprints are preliminary reports that have not undergone peer review.
They should not be considered conclusive, used to inform clinical practice,
or referenced by the media as validated information.

Development of a biomimetic hydrogel cervical spinal cord surrogate for transverse compression across loading rates

Paria Arjmandisarvestani
University of Strathclyde https://orcid.org/0009-0001-7680-9274
Nicholas Cunha
Adelaide University https://orcid.org/0009-0003-4350-3783
Parham Foroutan
Adelaide University https://orcid.org/0000-0002-0510-8518
Yue Hui
Adelaide University https://orcid.org/0000-0002-1057-5671
Ashish Diwan
Adelaide University https://orcid.org/0000-0003-1037-8421
Ryan David Quarrington
ryan.quarrington@adelaide.edu.au
Adelaide University https://orcid.org/0000-0002-0633-2482

Research Article

Keywords: spinal cord surrogate, hydrogel, transverse compression, dynamic loading, double-network, biomechanics

Posted Date: July 23rd, 2026

DOI: https://doi.org/10.21203/rs.3.rs-10440572/v1

License: This work is licensed under a Creative Commons Attribution 4.0 International License.
Read Full License

Additional Declarations: The authors declare no competing interests.

Abstract

Study Design:

Experimental laboratory study; fully factorial hydrogel formulation design with mechanical benchmarking against published spinal cord tissue data.

Objectives

To develop and characterise polyacrylamide-alginate (PAAm-alginate) double-network hydrogels as surrogates for the transverse compressive response of cervical spinal cord tissue, and to identify the formulation variables governing surrogate stiffness.

Setting:

University biomechanics laboratory, Adelaide, Australia.

Methods

Twenty-seven formulations combined three alginate concentrations (4.7, 7.8, 10.3% w/v), three ionic crosslinkers ($CaCl_2$, $FeCl_3$, $AlCl_3$) and three immersion durations (1, 2, 3 h). 313 elliptical specimens were tested in transverse compression at four displacement rates (~ 0.01 to 140 s^{-1}). Characteristic curves were generated by arc-length re-parameterisation, compared by statistical parametric mapping, and benchmarked against published human and porcine cervical cord data.

Results

All formulations showed J-shaped, rate-dependent viscoelastic responses. Crosslinking ion valency had the greatest influence, trivalent species being approximately five times stiffer than divalent $CaCl_2$; alginate concentration had a moderate, diminishing effect and immersion duration had little effect beyond 2 h. $CaCl_2$ formulations matched the benchmarks most closely at every rate; at ~ 50 s^{-1}, $CaCl_2$ / 10.3% / pooled 2 h + 3 h matched porcine cervical cord in tangent modulus (~ 1180 kPa) and stress at benchmark failure strain (~ 490 kPa).

Conclusions

PAAm-alginate double-network hydrogels reproduce the nonlinear, rate-dependent transverse compressive behaviour of cervical spinal cord tissue and can be tuned to published benchmarks, most

closely under dynamic loading. They provide a basis for instrumentable cord surrogates for *ex vivo* injury biomechanics and surgical simulation.

Sponsorship:

University of Adelaide Medical School Development Grant.

Introduction

Traumatic spinal cord injury affects approximately 0.9 million people each year, and the cervical region accounts for most cases[1]. Neurological damage arises principally from direct mechanical insult to neural tissue during vertebral fracture, disc herniation, or retropulsion of bone into the spinal canal[2]. Understanding the conditions that initiate and propagate that damage therefore requires accurate physical representation of the cord itself, and not only of the surrounding spinal column.

Cadaveric experiments remain the principal means of quantifying cervical spine load transfer, intervertebral kinematics, and the structural thresholds associated with instability[3]. These models cannot currently measure what happens to the cord, because no mechanically representative surrogate exists that can be instrumented to record cord deformation and internal stress during simulated traumatic loading. The same gap constrains surgical simulation; contemporary cervical spine simulators reproduce procedural anatomy and assess operative performance, but do not provide biofidelic measurement of the mechanical exposure imposed on the cord[4]. Trainees consequently receive feedback on bone removal or instrument handling without objective indication that a manoeuvre has compressed, displaced, or stretched the cord to potentially unsafe levels. An instrumentable, mechanically faithful surrogate would serve both applications, enabling real-time quantification of cord deformation during traumatic loading, decompression, and instrumentation.

Spinal cord tissue exhibits a nonlinear, viscoelastic response under both tensile and transverse compressive loading, with a low-stiffness toe region followed by progressive stiffening prior to failure[5–7]. Both tangent modulus and stress at a given strain increase with loading velocity[6, 8]. This rate sensitivity is clinically relevant, since retropulsion of bone during burst fracture has been estimated to occur at velocities of up to 4.5 m/s, generating strain rates well above those used in most quasi-static testing protocols[6, 9]. Published tissue datasets are, however, heterogeneous; modulus varies with cord region and with age[6, 10], and reported values differ further with species, preparation, hydration, temperature, post-mortem interval, loading mode, and the mechanical parameters reported[11]. Surrogate design therefore requires interpretation across datasets rather than replication of any single one. Existing surrogates have relied largely on silicone elastomers, which are dimensionally stable and readily manufactured but do not reproduce the hydrated, strain-stiffening, viscoelastic behaviour of neural tissue[12, 13].

Hydrogels are a more promising basis for cord surrogates, because their high water content, soft tissue-like deformability, and tunable mechanical properties resemble neural tissue more closely than elastomers[14]. Double-network architectures, including alginate-polyacrylamide systems, combine large-strain deformability with improved toughness, allowing constructs to withstand handling and repeated compression while remaining hydrated and compliant[15, 16]. Ionic crosslinking of the alginate network, with the covalent polyacrylamide network providing structural support, allows stiffness to be tuned through alginate concentration, crosslinking ion, and conditioning protocol[15–17]. Hydrogels have been examined extensively as drug delivery matrices and cell scaffolds for spinal cord repair, where their biocompatibility, injectability and tuneable degradation kinetics are established[14, 18], but their use as mechanically faithful physical surrogates remains comparatively underdeveloped, particularly for applications requiring direct measurement of cord deformation. This is most relevant in the cervical spine, where traumatic injury is common, degenerative cervical myelopathy frequently involves cord compression and surgical decompression, and cervical-specific mechanical datasets are available for surrogate validation.

This study aimed to develop and characterise PAAm-alginate double-network constructs capable of reproducing the transverse compressive response of the cervical spinal cord across strain rates relevant to traumatic and surgical loading, and to determine how formulation and immersion conditioning influence that response. We hypothesised that crosslinking ion valency would exert a greater influence on surrogate stiffness than either alginate concentration or immersion duration; that all formulations would display J-shaped, rate-dependent viscoelastic behaviour analogous to cord tissue; and that at least one formulation would fall within the reported variability of cervical cord tissue at each benchmarked loading rate.

Methods

Specimen fabrication

PAAm-alginate double-network surrogate cords were fabricated using a synthesis strategy adapted from Sun et al.[16], with alginate concentration, ionic crosslinking species, and immersion duration systematically varied (Fig. 1). Sodium alginate (FMC Biopolymer, LF 20/40) and acrylamide monomer (Sigma-Aldrich, A8887) were dissolved together in deionised water at alginate concentrations of 4.7, 7.8, and 10.3% w/v, with acrylamide concentration held constant across formulations. Ammonium persulphate (Sigma-Aldrich, A9164) was added as the radical initiator and N,N′-methylenebisacrylamide (MBAA; Sigma-Aldrich, M7279) as the covalent crosslinker, each at 2 wt% of the acrylamide monomer mass. Following degassing under vacuum for 15 min, N,N,N′,N′-tetramethylethylenediamine (TEMED; Sigma-Aldrich, T7024) was added as the polymerisation accelerator at 0.25 wt% of the acrylamide monomer mass. The precursor solution was cast into custom 3D-printed elliptical moulds dimensioned to replicate the human cervical spinal cord cross-section (transverse diameter 13 mm, anteroposterior diameter 8 mm, length 100 mm)[19].

Following initial gelation, the alginate network was ionically crosslinked by immersion in 0.1 M aqueous $CaCl_2$, $FeCl_3$ or $AlCl_3$ for 1, 2 or 3 h, yielding a fully factorial design of 27 formulations (Fig. 1). Constructs were then transferred to phosphate-buffered saline (PBS) for 24 h prior to testing, to approximate the aqueous conditioning environment of *ex vivo* cadaveric experiments[17]. Specimens were equilibrated at room temperature for 2 h and sectioned transversely into five 20 mm test segments immediately before testing.

Mechanical testing

Two testing platforms were used to span the strain rates relevant to physiological and traumatic cord loading (Fig. 1). Specimens were randomly assigned to one of four displacement rates: 0.1 mm/s (~ 0.01 s^{-1}) and 3.6 mm/s (~ 0.5 s^{-1}) on a uniaxial material testing machine (Instron 5543, Norwood, MA, USA), and 360 mm/s (~ 50 s^{-1}) and 1000 mm/s (~ 140 s^{-1}) on a drop tower comprising a guided carriage released from a prescribed height by an electromagnetic release mechanism. Specimens were positioned on a flat horizontal platen with the longitudinal axis perpendicular to the loading direction. Loading rates, boundary conditions and impactor geometry (5 mm diameter cylindrical flat end) were matched to previous transverse compression studies of human and porcine cord tissue to permit direct comparison[6, 20]. During quasi-static testing, force was recorded with the integrated ± 50 N load cell and crosshead displacement with the built-in linear variable differential transducer, both at 100 Hz. During dynamic testing, force was recorded with a six-axis load cell (± 440 N; MC3A-6-100, AMTI, MA, USA) nominally at 10 kHz, with the exception of 18 tests sampled at 5 kHz, and indenter displacement was determined from synchronised high-speed video (10 kHz; VEO1010, Phantom, Vision Research, NJ, USA).

Data processing

Force-time and displacement-time records were processed using custom code in MATLAB (R2026a, MathWorks, MA, USA). Detailed analysis methods are described in full in Supplementary Methods. Briefly, drop-tower data were aligned on a common trigger signal and the impact window isolated using a two-stage threshold applied to the smoothed post-trigger force signal; final force data were filtered using an SAE J211 CFC 1000 Butterworth filter. Because high-speed video displacement data were pixel-quantised, multi-stage polynomial fitting was used to recover a smooth force-displacement curve. Displacement was zeroed at first contact. Engineering strain was calculated as $\varepsilon = d / d_0$, where d is indenter displacement and d_0 the initial anteroposterior diameter (8 mm), and nominal stress as measured force divided by the initial projected contact area[6]. Curves were cropped from loading onset to specimen failure, defined by a distinct drop in force, and reviewed manually for data anomalies.

Statistical analysis

Stress-strain responses were analysed within each formulation and loading-rate group using arc-length re-parameterisation and characteristic response generation (ARCGen), which accommodates nonlinear curve shape, variable curve length, and inter-specimen variability[21]. ARCGen generated characteristic mean curves with ± 1 standard deviation corridors for each group. The effect of each formulation parameter was assessed by comparing characteristic responses across immersion duration, crosslinking ion, alginate concentration, and loading rate. Where levels of a parameter did not differ significantly, those levels were pooled to reduce redundancy and improve group-level estimates. Comparisons used one-dimensional statistical parametric mapping within the multivariate hypothesis-testing framework of Hartlen and Cronin[22], with Šidák-corrected Hotelling's T^2 tests and family-wise $\alpha = 0.05$. Implementation detail is provided in Supplementary Methods.

Benchmark comparison

Mechanical fidelity was assessed by comparing hydrogel characteristic curves with published cervical cord tissue data from Karimi et al.[20] and Fradet et al.[6]. Benchmark curves were digitised from the original publications and are therefore proxies rather than exact reproductions; variability bounds were available only for Fradet et al. Comparisons were rate-matched, using Karimi et al. for Speed 1 (0.01 s^{-1}) and the two Fradet et al. datasets for Speed 2 (0.5 s^{-1}) and Speed 3 (50 s^{-1}). Hydrogel curves were cropped to the strain range of the corresponding benchmark, with the Fradet et al. comparisons cropped at the reported mechanical failure strains of $\varepsilon = 0.74$ and $\varepsilon = 0.67$. Agreement was assessed by visual comparison of curve shape and by the mean squared residual (MSR) between each formulation curve and the benchmark. Following the method of Fradet *et al.*[6], tangent modulus was calculated from the longest segment ending at the benchmark failure strain for which a first-order linear fit achieved $R^2 \geq 0.99$, with a minimum window length of 10% of the strain range, and the same procedure was applied to the benchmark curves. Throughout, stiffness is used qualitatively to describe higher stress at equivalent strain, whereas tangent modulus refers to the slope-based measure. Normalisation and window-search procedures are detailed in Supplementary Methods.

Results

In total, 313 specimens were fabricated and tested across the 27 formulations, with five replicates per group for the $AlCl_3$ / 4.7% alginate formulations at Speeds 1 and 2 and three replicates for all remaining groups. Four specimens were excluded because of technical failures during testing, leaving 309 valid stress-strain curves (Supplementary Table S1). Initial analysis showed no significant difference between the 2 h and 3 h immersion groups, which were therefore pooled and are reported as the 2 h + 3 h pooled group. Individual specimen curves clustered closely within formulation groups (Supplementary Figures S4-S38; Fig. 2), supporting reproducible mechanical behaviour across specimens prepared identically.

Crosslinking agent had the largest influence on mechanical response, followed by alginate concentration, loading rate, and immersion duration. Trivalent agents produced the stiffest constructs,

with divalent $CaCl_2$ substantially more compliant and the responses diverging progressively at higher strains. $FeCl_3$ showed a stiffer toe region than $AlCl_3$, with the curves reconverging before $AlCl_3$ reached the higher tangent modulus at large strain. Statistical parametric mapping showed trivalent and divalent responses to be distinguishable across most of the strain range, whereas the two trivalent species differed only between approximately 0.25 and 0.8 strain (Supplementary Figure S2). Crosslinker effects were resolvable in all but one condition in the pooled 2 h + 3 h group and in 22 of 33 conditions at 1 h, with most exceptions in $AlCl_3$ versus $FeCl_3$ and Speed 4 comparisons (Supplementary Table S3).

Stiffness increased with alginate concentration across all crosslinking agents, with a diminishing effect at higher concentrations; the increment from 4.7 to 7.8% produced a consistently larger increase than that from 7.8 to 10.3%, particularly at lower loading speeds (Fig. 2). Concentration effects were detectable in 30 of 36 conditions in the pooled group and in 13 of 33 at 1 h, with most exceptions between 7.8 and 10.3% (Supplementary Table S4). Immersion duration had the smallest effect and was crosslinker dependent. $AlCl_3$ formulations were largely insensitive, with 1 of 12 conditions differing between 1 h and the pooled group, whereas $CaCl_2$ and $FeCl_3$ formulations stiffened beyond 1 h in 7 of 11 and 9 of 12 conditions respectively (Fig. 2; Supplementary Table S2).

All formulations stiffened with increasing displacement rate, the stress-strain curve shifting upward at each successive speed (Fig. 2). This was resolvable across all 54 pairwise speed comparisons in the pooled group and in 31 of 45 at 1 h, with exceptions concentrated in $AlCl_3$ formulations at 7.8 and 10.3% alginate and in Speed 1 versus Speed 2 comparisons (Supplementary Table S5). Peak stress increased progressively with rate, apart from a transient decrease between Speed 2 and Speed 3 that coincided with the change in testing apparatus and does not reflect a material characteristic.

All formulations reproduced the J-shaped characteristic curve of biological tissue (Fig. 3). $CaCl_2$ formulations gave the closest match at every benchmarked rate, with trivalent agents substantially stiffer than the tissue benchmarks (Supplementary Figure S3). The closest individual proxies were $CaCl_2$ / 4.7% / 1 h for Speed 1, $CaCl_2$ / 7.8% / 1 h for Speed 2, and $CaCl_2$ / 10.3% / pooled 2 h + 3 h for Speed 3 (Table 1; Fig. 3). For Speed 1, the benchmark strain range fell within the low-stiffness toe region of the $CaCl_2$ characteristic curve, resulting in the appearance of an approximately linear hydrogel response within that window, rather than J-shaped. Quantitative properties for all formulations and benchmarks across the three loading speeds are summarised in Supplementary Table S6.

Table 1

Summary of benchmark comparisons between hydrogel surrogate formulations and published cervical spinal cord tissue data at three loading rates. Tangent modulus was determined over the longest strain segment ending at the benchmark failure strain for which a first-order fit achieved $R^2 \geq 0.99$. Stress is reported at the benchmark failure strain. The best-matching formulation at each rate was identified by minimum mean squared residual against the benchmark curve.

Loading rate	Benchmark dataset*	Comparison failure strain	Best-matching formulation	Tangent modulus, surrogate vs benchmark (kPa)	Stress at failure strain, surrogate vs benchmark (kPa)
Speed 1 (0.01 s^{-1})	Karimi *et al.*	~ 0.25	$CaCl_2$ / 4.7% / 1 h	150.4 ± 5.1 vs 878.3	40.4 ± 1.1 vs 61.2
Speed 2 (0.5 s^{-1})	Fradet *et al.*	0.74	$CaCl_2$ / 7.8% / 1 h	528.4 ± 67.9 vs 591.7	252.9 ± 15.9 vs 251.0 ± 46.5
Speed 3 (50 s^{-1})	Fradet *et al.*	0.67	$CaCl_2$ / 10.3% / pooled 2 h + 3 h	1183.0 ± 192.3 vs 1176.2	490.1 ± 58.9 vs 458.7 ± 258.5

*Benchmark values were calculated from the manuscript's exemplar stress-strain figure.

Discussion

All 27 formulations exhibited a nonlinear, viscoelastic, J-shaped response, with a low-stiffness toe region at small strains followed by progressive strain-stiffening. This behaviour was consistent across alginate concentrations, ion species, immersion durations, and loading rates, and parallels the response of spinal cord tissue under transverse compression[5, 6]. PAAm-alginate double-network hydrogels are therefore a mechanically appropriate material platform for spinal cord surrogates. The hydrogels also demonstrated high tunability. For example, formulations spanned tangent moduli of approximately 150 to 1400 kPa at Speed 1 (Supplementary Table S6), a range that silicone-based surrogates do not provide[12]; those materials replicate only the low-strain modulus of cord tissue and lack the rate-dependent nonlinearity required for biomechanical fidelity.

The dominant influence of crosslinking ion valency is consistent with the coordination chemistry of the respective cations[17]. Al^{3+} and Fe^{3+} interact with both M- and G-block residues of the alginate backbone, generating a substantially denser network than Ca^{2+}, which binds only G-block segments through the egg-box mechanism[17]. Trivalent formulations accordingly produced stresses approximately five times those of $CaCl_2$ across the strain range. That $FeCl_3$ produced a stiffer toe region than $AlCl_3$ while converging at higher strain indicates that varying the ion within a valency tunes distinct features of the curve, allowing the toe region to be adjusted with comparatively little change to the linear region. This is directly useful for surrogate design, since the toe region governs the response to low-level contact during surgical manipulation, whereas the linear region governs the response during severe compression.

Increasing alginate concentration raised stiffness across all ion types, reflecting the higher crosslink density achievable at elevated polymer content[17], but with diminishing returns above 7.8%. A plausible explanation is the fixed 0.1 M crosslinker concentration used across formulations; as polymer content rises, the molar ratio of available ions to polymer binding sites falls, and alginate crosslinking depends strongly on the cation-to-guluronate ratio that governs the formation and propagation of ionic junction zones[23]. Available ions may therefore have been insufficient to crosslink a proportionate number of binding sites within the fixed immersion period. This remains an interpretation rather than a demonstrated mechanism; direct measurement of ion uptake would be required to confirm it. Immersion duration had the smallest effect, with little change beyond 2 h but consistent stiffening between 1 h and the pooled 2 h + 3 h group, indicating early time-dependent maturation of the ionic network. The rapid stabilisation of $AlCl_3$ is consistent with an early binding equilibrium or an early-stage diffusion barrier, whereas the more gradual maturation of the $CaCl_2$ and $FeCl_3$ networks suggests progressive internal diffusion and reorganisation of ions within the matrix[24]. Fewer significant differences were detected at 1 h across all comparisons, which reflects both reduced statistical power relative to the pooled group and genuinely higher intra-group variability in incompletely crosslinked networks. Practically, mechanical properties continue to evolve at short immersion times, so minor differences in handling time between specimens introduce variability; fixing immersion duration and varying ion concentration instead is more likely to yield homogeneous, fully equilibrated constructs.

Rate-dependent stiffening was observed in all formulations, qualitatively replicating the strain-rate sensitivity of spinal cord tissue reported by Fradet et al.[6] and Fiford and Bilston[8]. The transient decrease in peak stress between Speed 2 and Speed 3 is best explained as an apparatus artefact; unlike a materials testing machine, which supplies energy throughout loading, a drop tower delivers a fixed quantity of kinetic energy that is progressively dissipated, and localised puncturing of the specimen by the high-velocity impactor is also likely to have contributed. This should be considered when interpreting absolute stress magnitudes across the quasi-static to dynamic transition.

$CaCl_2$-crosslinked formulations corresponded most closely to native cervical cord at all three benchmarked rates, with $AlCl_3$- and $FeCl_3$-crosslinked formulations consistently exceeding the biological reference stiffness. At 0.1 mm/s, $CaCl_2$ / 4.7% / 1 h most closely matched the human cervical cord data of Karimi et al.[20]. However, this comparison is limited because the benchmark extends only to ~ 0.25 strain, compared with ~ 0.8 for the hydrogels; consequently, only the near-linear portion of the surrogate response is captured within the benchmark range. At 3.6 mm/s, $CaCl_2$ / 7.8% / 1 h best matched porcine cervical cord at 0.5 s^{-1}[6], although the curve trajectories differed; the tissue benchmark has a prolonged compliant toe extending to approximately 0.3 strain followed by a steep J-shaped rise, whereas the hydrogel grows more gradually, producing a crossover near 0.5 strain. Correspondence was strongest under dynamic impact. At 360 mm/s (~ 50 s^{-1}), the $CaCl_2$ / 10.3% / pooled 2 h + 3 h formulation followed the high-rate porcine benchmark closely and overlapped its reported variability, with a tangent modulus of approximately 1180 kPa and a stress of approximately 490 kPa at the benchmark failure strain of 0.64[6]. This is the loading regime of greatest relevance to injury biomechanics, where cord impingement

during high-energy cervical trauma may occur at velocities approaching 4.5 m/s. Rate-dependent stiffening continued at the highest rate tested (~ 140 s^{-1}), which is consistent with fluid-solid interaction in hydrated polymer networks, where rapid loading limits fluid redistribution and network relaxation[25]. Because native cord behaviour is poorly characterised at these rates, high-rate biological tissue data are needed to support surrogate validation in the conditions most relevant to severe traumatic cord impingement.

Several limitations apply. The hydrogel responses remained stiffer than the benchmarks at low to moderate strains, so further formulation optimisation is required to reproduce the compliant toe region of native cord tissue. The simplified elliptical geometry did not represent grey-white matter regional variation[26], the surrounding cerebrospinal fluid and dura, or canal constraint. Nominal stress calculated from projected contact area assumes a contact geometry that does not hold at large deformation[27]; contact-corrected analysis or inverse finite element modelling would be required to recover intrinsic material parameters. The biological comparators differ in species and testing configuration, combining human axial compression data[20] with porcine transverse compression data[6], so quantitative equivalence between surrogate and tissue should be interpreted cautiously. Finally, PBS conditioning was used to approximate the aqueous environment of *ex vivo* cadaveric experiments, but its influence on mechanical response requires direct quantification, because ionically crosslinked alginate networks can be altered by competitive ion exchange[17].

PAAm-alginate double-network hydrogels provide a tunable platform for biomimetic spinal cord surrogates with nonlinear, rate-dependent mechanical behaviour, and $CaCl_2$-crosslinked formulations correspond most closely to native cervical cord tissue among the agents tested. The formulation space should be extended to lower alginate concentrations and to alternative divalent ions such as Ba^{2+}, Sr^{2+} and Zn^{2+}, which produce distinct network architectures and mechanical responses in alginate hydrogels[28], and predictive models relating formulation to mechanical response would reduce the experimental burden of surrogate design. The immediate translational step is to combine anatomically realistic geometry with embedded sensing, producing a surrogate that reports cord deformation directly during simulated burst fracture, decompression, and instrumentation. Such a construct would allow *ex vivo* injury biomechanics experiments to measure the mechanical exposure of the cord rather than infer it, and would allow cervical spine surgical simulators to give trainees objective feedback on cord loading during high-risk manoeuvres.

Declarations

Ethical Approval

Ethical approval was not required for this study. The work involved mechanical testing of synthetic hydrogel constructs only; no human participants, human tissue, animals, or animal tissue were used. Biological comparison data were obtained from previously published studies.

Conflict of Interest Statement

The authors declare that no benefits in any form have been or will be received from a commercial party related directly or indirectly to the subject of this manuscript.

Funding statement

This work was supported by a University of Adelaide Medical School Development Grant.

Author Contribution

RDQ, PF, and AM conceived of, and designed, this study. RDQ, PF, and AM manufactured the specimens and performed the experiments. NC, RDQ, and PF performed the data analysis. NC, PA, YH, AD, and RDQ interpreted data. PA, NC, PF, and RDQ drafted the manuscript, and all authors provided critical revision.

Acknowledgments

The authors acknowledge Manpreet Pandher for assisting with mechanical testing and data analysis, and Devon Hartlen and Duane Cronin for their assistance with statistical analysis and interpretation.

Data Availability Statement

The processed stress-strain datasets and characteristic curves generated during this study are provided within the article and its supplementary files. Raw force-displacement records and the MATLAB analysis code are available from the corresponding author on reasonable request.

References

1. Safdarian M, Trinka E, Rahimi-Movaghar V, Thomschewski A, Aali A, Abady GG et al (2023) Global, regional, and national burden of spinal cord injury, 1990–2019: a systematic analysis for the Global Burden of Disease Study 2019. Lancet Neurol 22(11):1026–1047
2. Sekhon LH, Fehlings MG (2001) Epidemiology, demographics, and pathophysiology of acute spinal cord injury. Spine 26(24S):S2–S12
3. Nightingale RW, McElhaney JH, Richardson WJ, Best TM, Myers BS (1996) Experimental impact injury to the cervical spine: relating motion of the head and the mechanism of injury. JBJS 78(3):412–421
4. Weiss MY, Melnyk R, Mix D, Ghazi A, Vates GE, Stone JJ (2020) Design and validation of a cervical laminectomy simulator using 3D printing and hydrogel phantoms. Operative Neurosurg 18(2):202–208

5. Bilston LE (2011) Neural tissue biomechanics, vol 3. Springer Science & Business Media
6. Fradet L, Cliche F, Petit Y, Mac-Thiong J-M, Arnoux P-J (2016) Strain rate dependent behavior of the porcine spinal cord under transverse dynamic compression. *Proceedings of the Institution of Mechanical Engineers, Part H: Journal of Engineering in Medicine* ; 230(9): 858–866
7. Bilston LE, Thibault LE (1995) The mechanical properties of the human cervical spinal cord in vitro. Ann Biomed Eng 24(Suppl 1):67–74
8. Fiford RJ, Bilston LE (2005) The mechanical properties of rat spinal cord in vitro. J Biomech 38(7):1509–1515
9. Wilcox R, Allen D, Hall R, Limb D, Barton D, Dickson R (2004) A dynamic investigation of the burst fracture process using a combined experimental and finite element approach. Eur Spine J 13(6):481–488
10. Clarke EC, Cheng S, Bilston LE (2009) The mechanical properties of neonatal rat spinal cord in vitro, and comparisons with adult. J Biomech 42(10):1397–1402
11. Stanners M, O'Riordan M, Theodosiou E, Souppez J-BR, Gardner A (2024) The mechanical properties of the spinal cord: a systematic review. Spine J 24(7):1302–1312
12. Kroeker SG, Morley PL, Jones CF, Bilston LE, Cripton PA (2009) The development of an improved physical surrogate model of the human spinal cord—tension and transverse compression. J Biomech 42(7):878–883
13. Facchinello Y, Wagnac É, Ung B, Petit Y, Pradhan P, Peyrache L-M et al (2017) Development of an instrumented spinal cord surrogate using optical fibers: A feasibility study. Med Eng Phys 48(1):212–216
14. Haggerty AE, Oudega M (2013) Biomaterials for spinal cord repair. Neurosci Bull 29(4):445–459
15. Gong JP (2010) Why are double network hydrogels so tough? Soft Matter 6(12):2583–2590
16. Sun J-Y, Zhao X, Illeperuma WR, Chaudhuri O, Oh KH, Mooney DJ et al (2012) Highly stretchable and tough hydrogels. Nature 489(7414):133–136
17. Houben S, Pitet LM (2023) Ionic crosslinking strategies for poly (acrylamide)/alginate hybrid hydrogels. Reactive Funct Polym 191:105676
18. Peng H, Liu Y, Xiao F, Zhang L, Li W, Wang B et al (2023) Research progress of hydrogels as delivery systems and scaffolds in the treatment of secondary spinal cord injury. Front Bioeng Biotechnol 11:1111882
19. Ko H-Y, Park J, Shin Y, Baek S (2004) Gross quantitative measurements of spinal cord segments in human. Spinal Cord 42(1):35–40
20. Karimi A, Shojaei A, Tehrani P (2017) Mechanical properties of the human spinal cord under the compressive loading. J Chem Neuroanat 86:15–18
21. Hartlen DC, Cronin DS (2022) Arc-length re-parametrization and signal registration to determine a characteristic average and statistical response corridors of biomechanical data. Front Bioeng Biotechnol 10:843148

22. Hartlen DC, Cronin DS (2025) Hypothesis Testing of Multivariate Biomechanical Responses using Statistical Parametric Mapping and Arc-Length Re-parameterization: DC Hartlen, DS Cronin. Ann Biomed Eng 53(10):2536–2550
23. Ručigaj A, Golobič J, Kopač T (2024) The role of multivalent cations in determining the cross-linking affinity of alginate hydrogels: A combined experimental and modeling study. Chem Eng J Adv 20:100678
24. Chen C-K, Lin C-Y, Chakravarthy RD, Chen Y-H, Chen C-Y, Lin H-C et al (2025) Effect of metal ions on the conductivity, self-healing, and mechanical properties of alginate/polyacrylamide hydrogels. Materials 18(16):3871
25. Cheng S, Bilston LE (2007) Unconfined compression of white matter. J Biomech 40(1):117–124
26. Ichihara K, Taguchi T, Shimada Y, Sakuramoto I, Kawano S, Kawai S (2001) Gray matter of the bovine cervical spinal cord is mechanically more rigid and fragile than the white matter. J Neurotrauma 18(3):361–367
27. Finan JD, Fox PM, Morrison IIIB (2014) Non-ideal effects in indentation testing of soft tissues. Biomech Model Mechanobiol 13(3):573–584
28. Malektaj H, Drozdov AD, deClaville Christiansen J (2023) Mechanical properties of alginate hydrogels cross-linked with multivalent cations. Polymers 15(14):3012

Figures

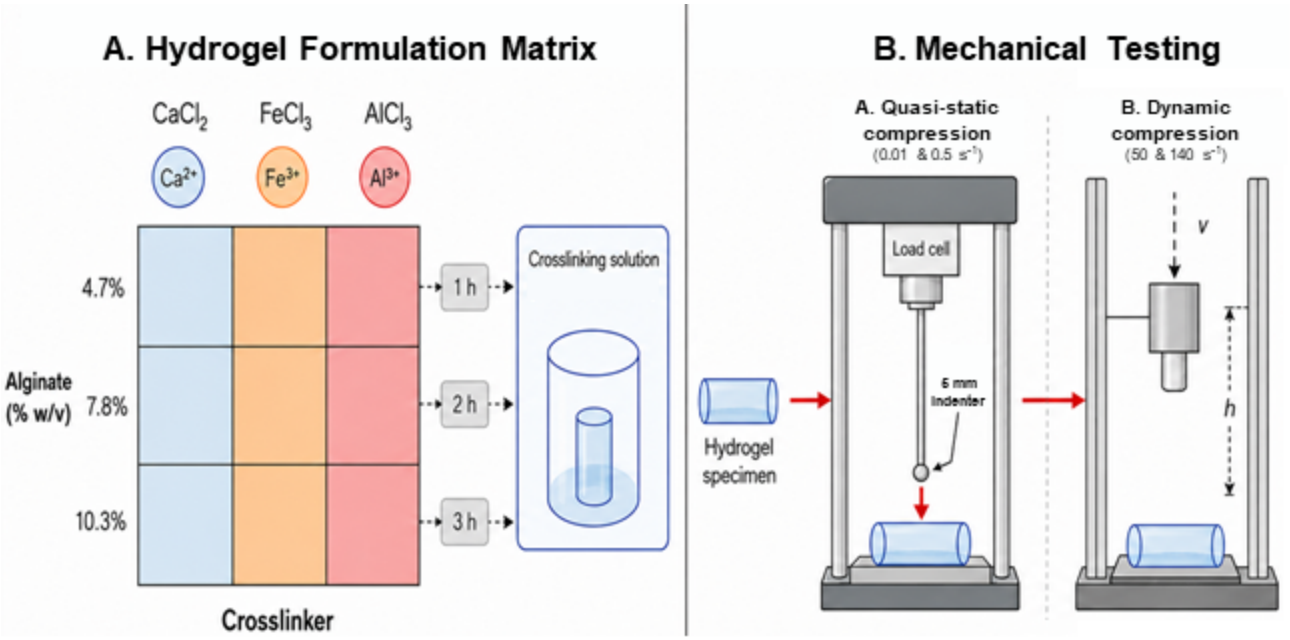


Figure 1

Graphical overview of the study design and mechanical testing workflow. (A) Fully factorial hydrogel formulation matrix (3 alginate concentrations × 3 crosslinking ions × 3 immersion durations); (B) transverse compression testing using a materials testing machine and drop tower.

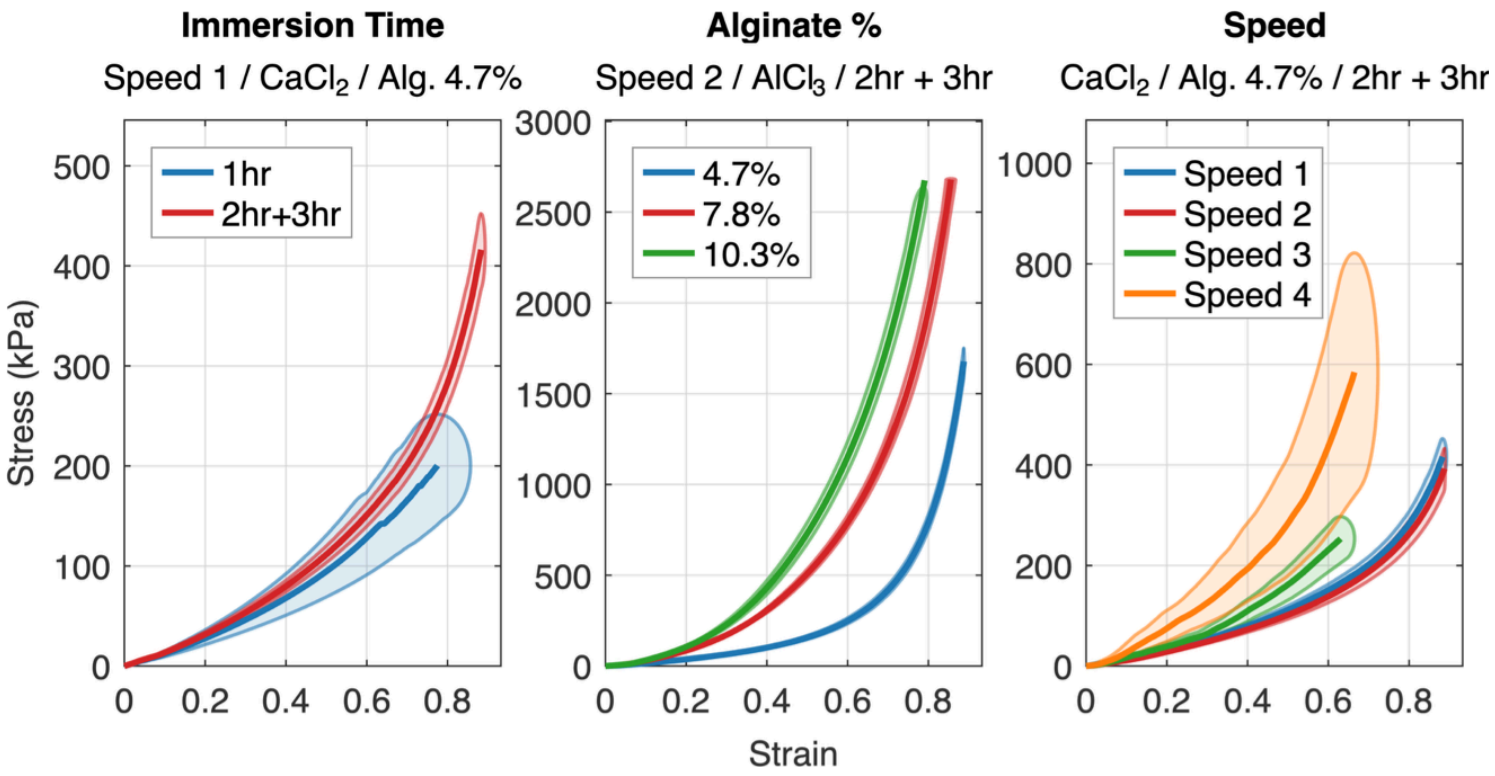


Figure 2

Characteristic stress-strain curves comparing, from left to right: immersion time (1 hr: n = 3, pooled 2+3 hr: n = 6; Speed 1, $CaCl_2$, 4.7% alginate), alginate concentration (4.7%: n = 10, 7.8%: n = 6, 10.3%: n = 6; Speed 2, $AlCl_3$, pooled immersion times), and speed (Speeds 1-4: n = 6 per speed; $CaCl_2$, 4.7% alginate, pooled immersion times). Solid lines represent characteristic curves and shaded envelopes denote ±1 standard deviation corridors.

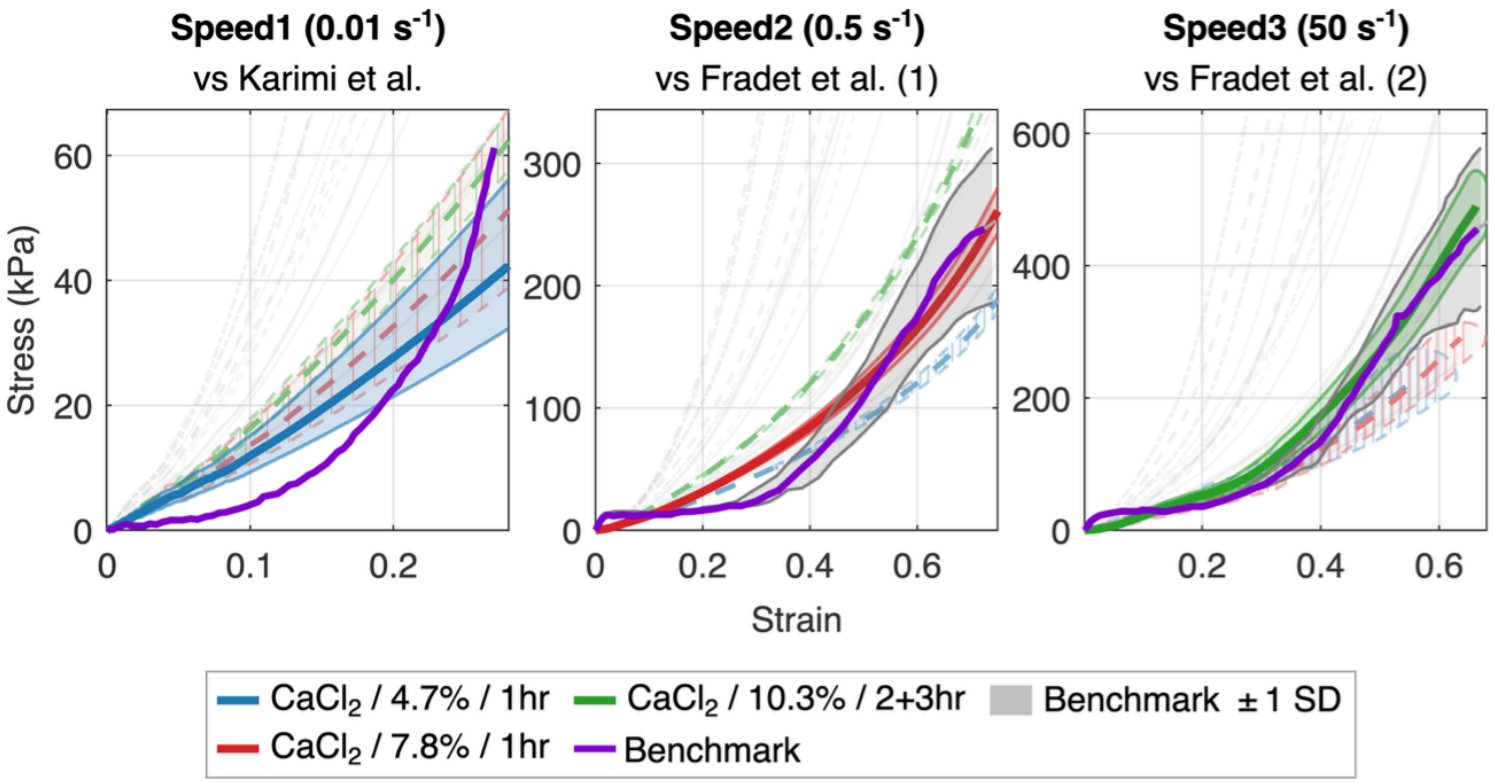


Figure 3

Characteristic stress-strain curves from all 18 hydrogel formulations (3 alginate concentrations × 3 crosslinking salts × 2 immersion time groups) compared against ex vivo spinal cord tissue benchmarks, from left to right: Speed 1 (0.01 s^{-1}) vs Karimi et al., Speed 2 (0.5 s^{-1}) vs Fradet et al. (1), and Speed 3 (50 s^{-1}) vs Fradet et al. (2). In each panel, the best-matching formulation for that speed, identified by minimum mean squared residual (MSR) against the benchmark, is shown as a solid coloured line with a shaded ±1 SD corridor; the best-matching formulations from the other two speeds are shown as dashed lighter lines with hatched corridors; all remaining formulations are shown as faint grey lines. The benchmark mean curve is shown in purple; grey shaded corridors represent published ±1 SD bounds (Fradet panels only). Best-matching formulations: Speed 1, $CaCl_2$, 4.7% alginate, 1 hr immersion; Speed 2, $CaCl_2$, 7.8% alginate, 1 hr immersion; Speed 3, $CaCl_2$, 10.3% alginate, pooled 2+3 hr immersion. Benchmark curves were digitised manually from published figures and are presented for illustrative comparison only.

Supplementary Files

This is a list of supplementary files associated with this preprint. Click to download.

- SupplementaryMaterialv7.docx